MATERIALS SCIENCE

Molecular beam homoepitaxy of N-polar AlN: Enabling role of aluminum-assisted surface cleaning

Zexuan Zhang[1]*, Yusuke Hayashi[2], Tetsuya Tohei[2], Akira Sakai[2], Vladimir Protasenko[1], Jashan Singhal[1], Hideto Miyake[3,4], Huili Grace Xing[1,5,6], Debdeep Jena[1,5,6], YongJin Cho[1]*

N-polar aluminum nitride (AlN) is an important building block for next-generation high-power radio frequency electronics. We report successful homoepitaxial growth of N-polar AlN by molecular beam epitaxy (MBE) on large-area, cost-effective N-polar AlN templates. Direct growth without any in situ surface cleaning leads to films with inverted Al polarity. It is found that Al-assisted cleaning before growth enables the epitaxial film to maintain N-polarity. The grown N-polar AlN epilayer with its smooth, pit-free surface duplicates the structural quality of the substrate, as evidenced by a clean and smooth growth interface with no noticeable extended defects generation. Near band-edge photoluminescence peaks are observed at room temperature on samples with MBE-grown layers but not on the bare AlN templates, implying the suppression of nonradiative recombination centers in the epitaxial N-polar AlN.

INTRODUCTION

High–electron-mobility transistors (HEMTs) built on wide-bandgap semiconductor material platforms such as III-nitrides are leading contenders in high-power, millimeter-wave electronics (*1*–*3*). Compared with their metal-polar counterparts, N-polar GaN-based HEMTs allow for the simpler formation of low-resistance contacts due to the absence of a top barrier and a stronger carrier confinement thanks to the inherent back barriers (*4*, *5*). Current state-of-the-art performance has been achieved using N-polar GaN/AlGaN HEMTs with output powers above 8 W/mm at up to 94 GHz (*2*). The performance of N-polar III-N HEMTs can potentially be further improved with binary aluminum nitride (AlN) buffer layers (*6*, *7*). Because of its large bandgap (6 eV) and high thermal conductivity (~340 W/mK), AlN provides an unmatched combination of high electrical resistivity and thermal conductivity in the nitride semiconductor family (*1*, *8*). As a result, incorporating free-standing N-polar AlN as the buffer layer for N-polar III-N HEMTs has the advantages of enhanced thermal management and a maximized conduction band offset to help reduce buffer leakage and short channel effects (*1*, *5*–*7*, *9*). In addition, substituting the AlGaN buffer layer with AlN can induce a higher density of two-dimensional electron gas (2DEG), can suppress alloy scattering, and has the potential to further boost the conductivity of the 2DEG channel (*5*–*7*, *10*). Moreover, III-N HEMTs on AlN can take advantage of the unprecedented level of integration in nitride electronics provided by the AlN platform (*1*).

The first step to achieve N-polar III-N HEMTs based on the AlN platform is the epitaxial growth of high-quality N-polar AlN. N-polar AlN has been synthesized on different foreign substrates such as Si, SiC, and sapphire using techniques such as metal-organic vapor phase epitaxy (MOVPE), sputtering, and molecular beam epitaxy (MBE) (*11*–*18*). Among these, optimal conditions for the MOVPE growth of N-polar AlN have been developed on C-face SiC substrates with an intentional miscut of 1° to achieve a smooth surface free of hexagonal hillocks and step bunching (*13*). This further led to the recent demonstration of N-polar AlGaN/AlN polarization-doped field-effect transistors (*9*). Yet to maximize the performance of such N-polar AlN-based devices, the development of a homoepitaxial growth technique on N-polar AlN substrate is highly desired. Reports on homoepitaxy of N-polar AlN, however, are rare. Although N-polar AlN homoepitaxy on single-crystal AlN substrates has been recently demonstrated by MOVPE (*14*), successful N-polar AlN homoepitaxy by MBE has not been reported yet.

In this work, we report the MBE homoepitaxy of N-polar AlN films on N-polar AlN templates. By comparing two samples with and without in situ Al-assisted surface cleaning of the substrate, we find Al-assisted surface cleaning to be crucial for achieving N-polarity of the MBE-grown AlN epilayers. The MBE-grown N-polar AlN is electrically insulating with a smooth pit-free surface and a high structural quality. No disordered interfacial layer or generation of extended defects is detected at the growth interface. In addition, near band-edge photoluminescence (PL) emission, absent from the bare substrate, is observed at room temperature on samples with MBE-grown layers.

RESULTS

Two samples with AlN layers grown by MBE on N-polar AlN templates are compared in this work. Except for the presence/absence of in situ Al-assisted surface cleaning before growth (as discussed later), the layer structures and growth conditions for the two samples are nominally identical. The inset of Fig. 1B shows a schematic of the sample structures used in this study. The difference between the two samples lies in the in situ surface cleaning before the MBE growth. For sample A, no intentional in situ cleaning was performed, whereas for sample B, Al-assisted surface cleaning was used before the MBE growth. The Al-assisted surface cleaning consists of multiple cycles of Al adsorption and desorption, similar to earlier reports on Al-polar AlN substrates (*19*, *20*). The substrate was first heated up to a thermocouple temperature of 1060°C without nitrogen

[1]School of Electrical and Computer Engineering, Cornell University, Ithaca, NY 14853, USA. [2]Graduate School of Engineering Science, Osaka University, 1-3 Machikaneyama-cho, Toyonaka, Osaka 560-8531, Japan. [3]Graduate School of Engineering, Mie University, 1577 Kurimamachiya-cho, Tsu, Mie 514-8507, Japan. [4]Graduate School of Regional Innovation Studies, Mie University, 1577 Kurimamachiya-cho, Tsu, Mie 514-8507, Japan. [5]Department of Materials Science and Engineering, Cornell University, Ithaca, NY 14853, USA. [6]Kavli Institute at Cornell for Nanoscale Science, Ithaca, NY 14853, USA.
*Corresponding author. Email: zz523@cornell.edu (Z.Z.); yongjin.cho@cornell.edu (Y.C.)

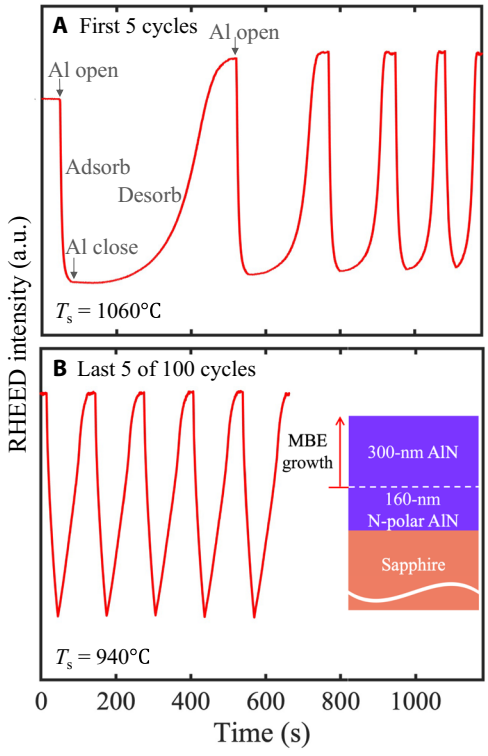

Fig. 1. RHEED intensity evolution during Al-assisted cleaning. (**A**) During the first five cycles at 1060°C and (**B**) during the last five cycles at 940°C. Inset: Schematic of the sample structures in this study. a.u., arbitrary units.

gas flow. During each Al adsorption/desorption cycle, the substrate was exposed to an Al flux with a beam equivalent pressure (BEP) of ~6 ×10^{-7} torr for 30 s. The Al shutter was then closed long enough for all of the deposited Al to desorb.

This Al adsorption and desorption process was clearly observed via the time evolution of the reflection high-energy electron diffraction (RHEED) intensity. Figure 1A shows the variation of the RHEED intensity during the first five Al-assisted cleaning cycles. As can be seen from Fig. 1A, the RHEED intensity drops when Al is deposited and gradually increases, eventually saturating, when it desorbs. Similar behavior was also observed for Al-polar AlN substrates (*19*, *20*). The time for the deposited Al to completely desorb from the surface (monitored by the saturation of RHEED intensity) monotonically decreases with an increasing number of Al-assisted cleaning cycles. The reason for the shortening of the Al desorption time is the gradual removal of surface oxide by Al metals, as has been explained in our previous work (*19*). During each Al-assisted cleaning cycle, the deposited Al metal reacts with the surface oxide to produce a volatile suboxide, which evaporates at high substrate temperature (*19*, *20*). Starting at a thermocouple temperature of 1060°C, Al-assisted cleaning cycles were repeated until the desorption time dropped below ~50 s, at which point the substrate temperature was lowered by 30°C; this process was then repeated until the substrate thermocouple temperature reached 940°C. This repeated temperature lowering was carried out to increase the lifetime of Al adatoms on the surface, providing them enough time to react with any residual surface oxides. To guarantee thorough surface oxide removal, a total of 100 Al-assisted cleaning cycles were performed. Concerning the number of cleaning cycles, it should be mentioned that the effectiveness of such Al-assisted cleaning is determined by both Al surface coverage and surface temperature, e.g., higher Al coverage on the surface, by either higher Al flux and/or longer Al deposition time, would lead to a smaller number of cleaning cycles to deoxidize a given N-polar AlN substrate, although then the desorption time (and the total time per cycle) would increase accordingly. Figure 1B shows the RHEED intensity versus time during the last five Al-assisted cleaning cycles at a lowered substrate temperature of 940°C. Almost no change in the evolution of the RHEED intensity is observed during these cycles, and we use this as an indicator of the surface being sufficiently cleaned (*19*). Note that the two-step adsorption/desorption process, which is characterized by a sharp change in the slope of RHEED intensity versus time [e.g., see figure 1 in (*19*)] and observed in an Al-polar AlN substrate due to a clear transition between adlayer and droplet formation/desorption (*19*, *20*), is not observed on the N-polar AlN template, indicating a relatively smaller diffusion length of Al adatoms on the N-polar AlN template surface.

The evolution of the RHEED patterns of both samples (viewed along the AlN <11$\bar{2}$0> azimuth) during the growth are displayed in Fig. 2. For sample A, the RHEED pattern was slightly diffused with faint streaks before growth (Fig. 2A). At the nucleation stage, the RHEED pattern became completely diffused (Fig. 2B), indicating a very high level of surface crystalline disorder. As growth proceeded, the RHEED pattern started to brighten, and streaks gradually recovered. Figure 2C shows the RHEED pattern by the end of the growth after desorption of excess Al droplets at 970°C. The bright and streaky RHEED pattern suggests a smooth surface. In contrast, the RHEED pattern for sample B before epitaxial growth (after Al-assisted cleaning) was bright and streaky (Fig. 2D). Such RHEED pattern persisted throughout the entire growth, as shown in Fig. 2 (E and F). No considerable change in the RHEED pattern was observed during cooling down the substrates to room temperature for both samples.

Examining the surface morphology of the two samples was done by atomic force microscopy (AFM). Although sample A has a smooth surface morphology with a low root mean square (RMS) roughness of 0.6 nm in a 10 μm × 10 μm, it has pits and trenches on the surface (Fig. 3, A and B). Apart from these features, clear atomic steps are observed, suggesting a step-flow growth mode enabled by Al-rich growth conditions. On the other hand, sample B is very smooth, with an RMS roughness as low as 0.3 nm in a 10 μm ×10 μm region (Fig. 3C). In addition, the 2 μm × 2 μm AFM scan in Fig. 3D shows the presence of smooth and parallel atomic steps. No visible hexagonal hillocks or surface pits were observed. The origin of the surface pits in sample A could be attributed to the relatively high-density contaminants including oxides, which are presumably present on the substrate surface due to the lack of any in situ surface cleaning. Similar pits have been found in films grown on N-polar GaN substrate with high-density C impurities on the substrate surface (*21*).

To determine the polarity of AlN layers, KOH etching is widely used, due to the substantially different etch rates for Al-polar and N-polar nitride surfaces (*13*, *22*, *23*). Specifically, Al-polar AlN exhibits defect-selective etch behavior by KOH with hexagonal pits generated around dislocations (*13*, *24*). In contrast, N-polar AlN can be etched by KOH with a much higher etch rate, with hexagonal pyramids bounded by more chemically stable {1$\bar{1}$0$\bar{1}$} crystallographic planes emerging after etching (*13*, *16*, *25*). Figure 4 shows the surface morphologies of both samples after etching in 50 weight %

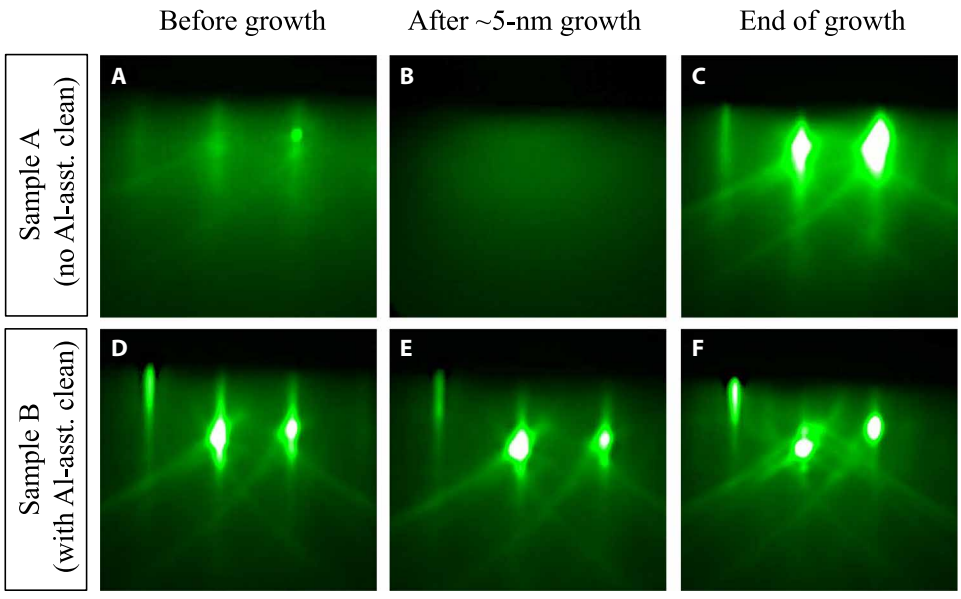

Fig. 2. Evolution of RHEED patterns during MBE growth of AlN. RHEED patterns taken before growth, after 5-nm growth, and by the end of growth of sample A (**A** to **C**) and sample B (**D** to **F**). All the RHEED patterns were taken along the AlN <11$\bar{2}$0> azimuth.

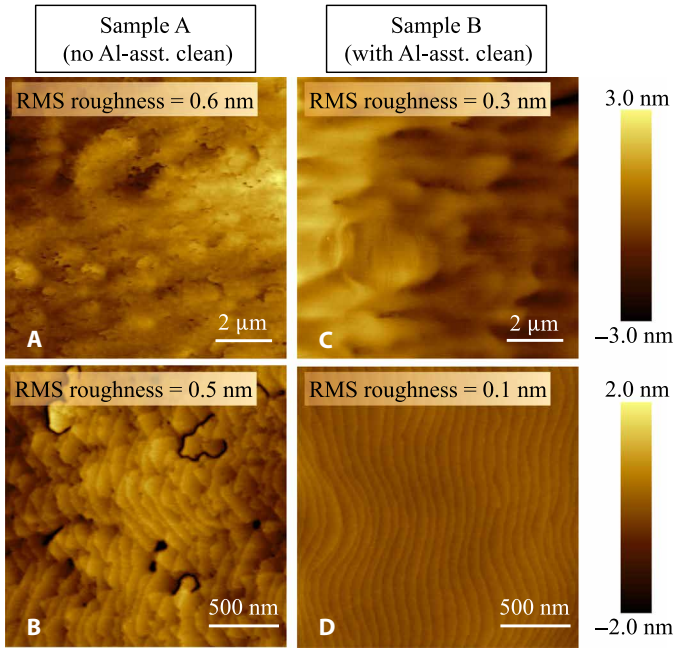

Fig. 3. Morphology of the as-grown surface of AlN. AFM micrographs (10 μm × 10 μm and 2 μm × 2 μm) of the surface of as-grown sample A (**A** and **B**) and sample B (**C** and **D**). Note that the pits and the trenches observed on sample A are absent on sample B.

KOH aqueous solution at room temperature for 10 min. Pits with a density of ~4×10^7 cm^{-2} were observed in a 5 μm × 5 μm AFM scan on sample A shown in Fig. 4A. A zoomed in 0.5 μm ×0.5 μm scan near a pit (the boxed region in Fig. 4A) further reveals its hexagonal shape (Fig. 4B) with a depth of ~120 nm (measured by a line scan along the white line). A schematic of sample A after KOH etch is shown in Fig. 4C. As mentioned earlier, such morphology after KOH etch is a signature of Al-polar AlN (*13*, *24*). In sharp contrast, sample B exhibits hexagonal pyramids after KOH etch, indicative of N-polarity, with a density of ~2×10^7 cm^{-2}, as can be seen in Fig. 4 (D and E). A line scan along the white line in Fig. 4E measures the height of the hexagonal pyramid to be ~150 nm. Figure 4F shows a schematic of sample B after etching in KOH. To further confirm the polarity of both samples, x-ray diffraction (XRD) and Raman spectroscopy were performed. Even after KOH etch, strong AlN peaks (marked by black dashed lines) with intensities comparable to those measured before KOH etch were seen on sample A in both XRD and Raman spectra (Fig. 5, A and B), indicating that the AlN film was not substantially etched by KOH and confirming that the film is Al-polar. For sample B, on the other hand, the AlN peaks in both the XRD and Raman spectra almost completely vanished after KOH etch, as indicated by the black arrows in Fig. 5 (C and D), verifying that the epitaxial film maintained the polarity of the N-polar substrate.

Scanning transmission electron microscopy (STEM) measurements were performed to study the atomic structure and directly probe the polarities of the MBE-grown AlN films in both samples. Figure 6A shows a bright-field (BF) cross-sectional STEM overview image of the cross section of sample A. An obvious interface structure marked by the white notches in Fig. 6A is seen between the sputtered N-polar AlN template and the MBE-grown layer, indicating that the AlN is structurally discontinuous across the interface region. In addition, the considerable image contrasts in the MBE-grown layer marked by the black triangles in Fig. 6A, which are absent in the substrate, are considered to be due to strain field from the extended defects generated near the growth interface during the MBE growth. These defects are further identified to be *a*-type dislocations, based on the BF-TEM images shown in the Supplementary Materials (fig. S1). The density of such dislocations obtained from plan-view TEM is ~2.6×10^{10} cm^{-2} (Fig. 7A), which is about one order higher than that in the AlN template estimated from the x-ray

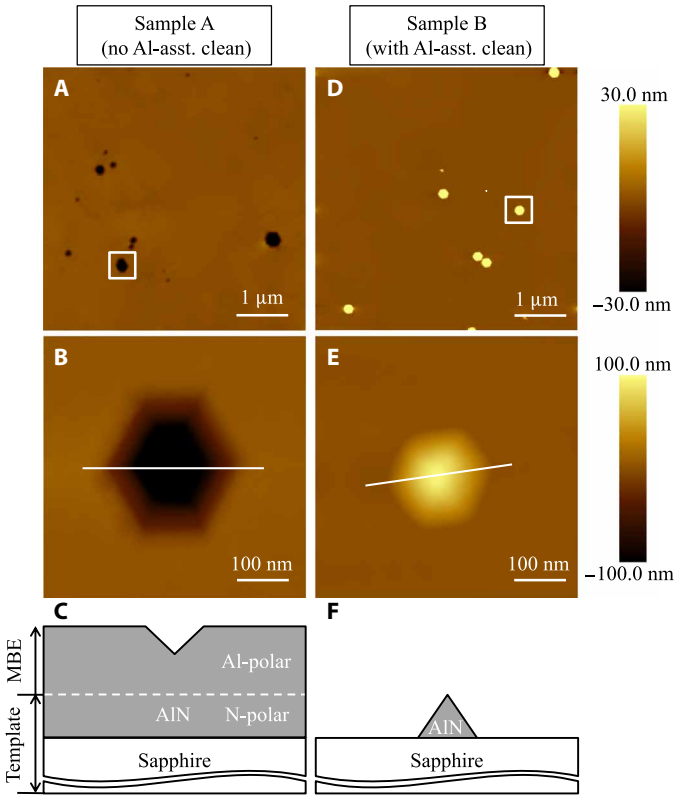

Fig. 4. Surface morphology of AlN after KOH etch. AFM micrographs (5 μm × 5 μm and 0.5 μm × 0.5 μm) and schematic after KOH etch of sample A (**A** to **C**) and sample B (**D** to **F**). Note the hexagonal pits (B) on sample A and the pyramids (E) on sample B after KOH etch, which are signatures of Al-polar and N-polar AlN surfaces, respectively.

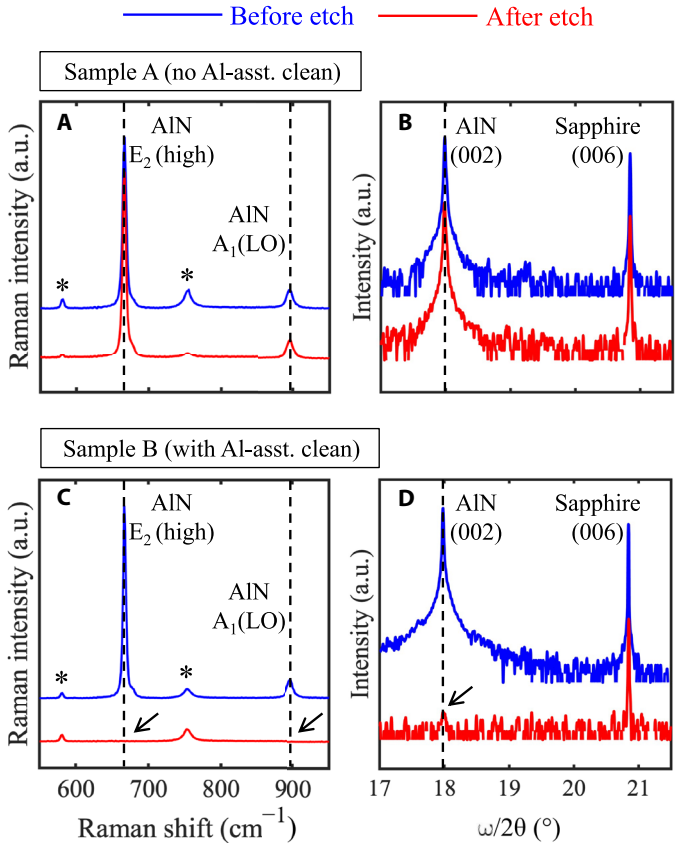

Fig. 5. Comparison of XRD and Raman spectra before and after KOH etch. Raman spectra and XRD ω/2θ scans of sample A (**A** and **B**) and sample B (**C** and **D**) before (blue lines) and after (red lines) KOH etch. The black dashed lines in (A) and (C) indicate the AlN Raman modes. Raman signals from the sapphire substrate are marked by the asterisks. Note that the AlN signals in sample B are almost completely vanished after KOH etch, as indicated by the black arrows in (C) and (D). a.u., arbitrary units.

rocking curves (XRCs) (*16*). Figure 6 (B to D) shows the magnified high-angle annular dark field STEM (HAADF-STEM) images of the corresponding regions marked by the black squares in Fig. 6A: Fig. 6B is taken close to the MBE-grown AlN surface, Fig. 6C shows the interface between sputtered and MBE-grown AlN, and Fig. 6D corresponds to the sputtered AlN/sapphire interface. Across a well-defined inversion domain boundary between the white dashed lines in Fig. 6C close to the growth interface, the AlN polarity is seen to be inverted from the N-polarity in the substrate (Fig. 6D) to the Al-polarity in the MBE-grown layer (Fig. 6B). This polarity inversion boundary shares a similar microstructure as the one previously reported in sputtered AlN films (*26*). On the contrary, the interface between the MBE-grown layer and the substrate in sample B is not visible in the BF-STEM overview image shown in Fig. 6E, suggesting a high level of structural continuity between the epilayer and the substrate across the interface. Unlike sample A, no sharp image contrast was detected in the MBE-grown layer across the STEM observation area. The structural continuity of the AlN in sample B can be further attested by plan-view TEM (Fig. 7B). The dislocation density of the MBE-grown AlN layer is ~1.8×10^9 cm^{-2}, which is very similar to that of the substrate (*16*). These dislocations are seen to be distributed along areal boundaries (see the red circles in Fig. 7B), which resembles misfit dislocations formed along grain boundaries at lattice-mismatched epitaxial films. On the basis of these observations, therefore, one can conclude that the MBE-grown AlN in sample B duplicated the microstructure of the underlying AlN on sapphire substrate with the dislocation density limited by that of the AlN template substrate, meaning high-quality homoepitaxy for sample B. Moreover, with Al-assisted cleaning before growth, the AlN layer in sample B maintains the polarity of the N-polar substrate, as evidenced by the magnified HAADF-STEM images taken within the MBE-grown AlN layer (Fig. 6F) and the substrate (Fig. 6H). As a result, no polarity inversion boundary is detected between the AlN layer and the substrate, as shown in Fig. 6G. By comparing the atomic structures of samples A and B, it is concluded that Al-assisted cleaning before growth is crucial to achieve a smooth interface and prevent polarity inversion during MBE homoepitaxy.

It is very likely that surface impurities such as O contribute to the polarity inversion of sample A. O has been found to play an important role in the polarity inversion from N-polar to Al-polar during AlN growth by other growth techniques including MOVPE and sputtering (*16*, *17*, *27*). For example, the polarity of AlN grown on the O plasma–treated N-polar AlN surface was found to be Al-polar (*27*). Besides, the atomic structure of the inversion domain boundary in Fig. 6C resembles the oxide inversion boundary with Al vacancies formed during sputtering deposition of AlN (*26*).

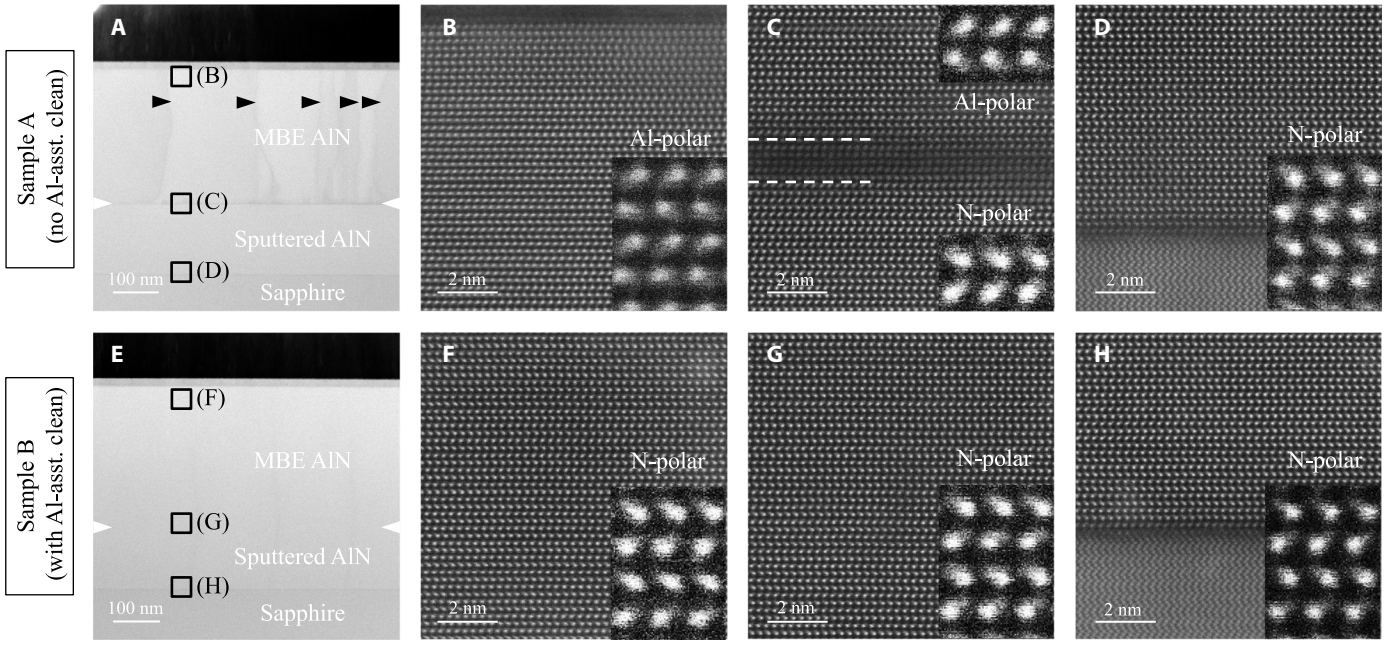

Fig. 6. Cross-sectional STEM images of MBE-grown AlN on AlN templates. Overview and magnified HAADF-STEM images of sample A (**A** to **D**) and sample B (**E** to **H**). The black squares in (A) and (E) mark the regions where the corresponding magnified images (B to D and F to H) are taken. The white notches in (A) and (E) indicate the growth interfaces. Note the considerable image contrasts in the MBE layer and at the growth interface in sample A (A) are absent in sample B (E).

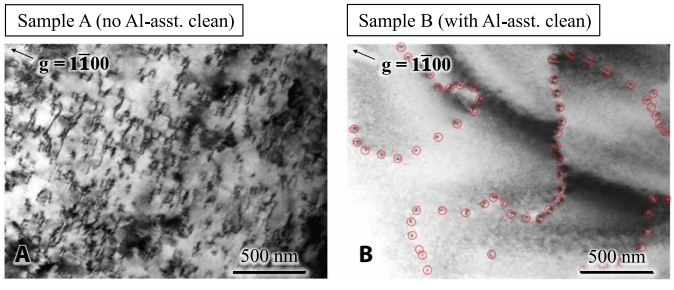

Fig. 7. BF plan-view TEM micrographs of MBE-grown AlN. The arrows indicate the diffraction vector $\mathbf{g} = 1\bar{1}00$ used for imaging the dislocations. The dislocation density is extracted to be ~2.6×10^{10} cm^{-2} for sample A (**A**) and ~1.8×10^{9} cm^{-2} for sample B (**B**). The circles in (B) indicate some of the dislocations.

To evaluate this hypothesis, secondary ion mass spectrometry (SIMS) characterization was conducted to study the impurity concentrations in both the samples. A large O spike with a peak concentration as high as ~6×10^{21} cm^{-3} was detected at the growth interface of sample A (Fig. 8A), while such a large O spike is completely absent at the growth interface of sample B (Figs. 8B), indicating that in situ Al-assisted cleaning is very effective in deoxidizing N-polar AlN substrates. For Si and H, both the samples show either doping level signals below 10^{19} cm^{-3} at the growth interfaces or densities close to the detection limits. While C concentration in the MBE-grown AlN is ~2×10^{17} cm^{-3} for sample A and close to the detection limit of 5×10^{16} cm^{-3} for sample B, it is seen that Al-assisted cleaning is not effective in removing C contaminants at the growth interfaces, which agrees with the case of Al-polar AlN (*19*). It is interesting that O shows a higher incorporation in the MBE-grown layer of sample B (~8×10^{17} cm^{-3}) than sample A (~3×10^{17} cm^{-3}). This could be due to the different polarities of the AlN films: Since the MBE-grown AlN is Al-polar for sample A and N-polar for sample B, the higher O level in sample B agrees with the previous studies, where O was found to incorporate more favorably in N-polar than Al-polar AlN (*28*, *29*).

Now, we compare the structural and optical properties between the MBE-grown (sample B) and sputter-deposited (bare substrate) N-polar AlN. The structural quality was evaluated by XRCs, i.e., ω scans. Figure 9 (A and B) shows the measured XRCs of sample B across the symmetric (0002) and skew-symmetric (10$\bar{1}$2) reflections, respectively. The full widths at half of maximum of the (0002) and (10$\bar{1}$2) peaks were extracted to be 14 and 380 arc sec, respectively. These values are very close to those [10/350 arc sec for (0002)/(10$\bar{1}$2) peak] measured on the AlN template substrates used in this study (*16*), suggesting again high-quality homoepitaxial growth of the N-polar AlN without noticeable additional generation of structural defects (see Fig. 6E).

Figure 9C compares the room temperature PL spectra of sample B and a bare substrate (after subtraction of background from sapphire) near the band-edge of AlN. While no near band-edge emission peak was detected on the bare AlN template, two emission peaks close to the band-edge of AlN were clearly observed on sample B. The emission peak with higher intensity is located at a photon energy of 5.98 eV, which is very close to the reported room temperature free exciton emission line (~5.96 eV) of Al-polar AlN epilayers and bulk AlN crystals (*30*, *31*), whereas the other emission peak at 5.84 eV likely originates from the electron-hole plasma recombination (~5.83 eV on bulk AlN crystals) (*31*). However, temperature- and excitation power-dependent PL measurements would be needed to uncover the origins of the PL peaks. Nevertheless, the observation of clear near band-edge PL emission from sample B, which is absent from the bare AlN template, indicates the suppression of nonradiative recombination centers in the MBE-grown N-polar AlN layer.

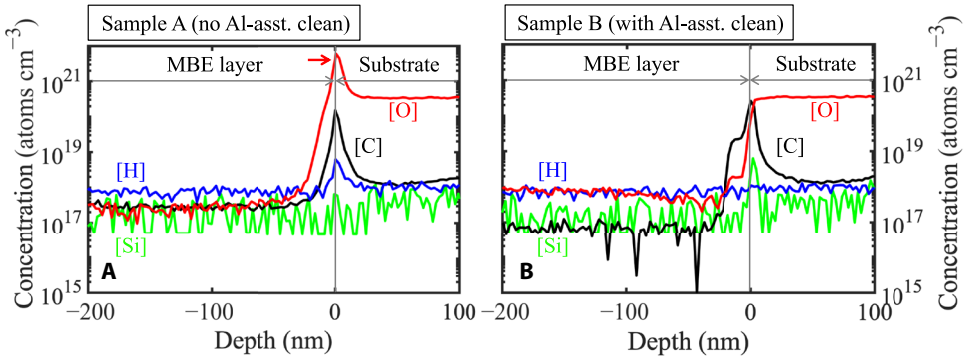

Fig. 8. SIMS depth profiles of O, C, Si, and H impurities. O (red), C (black), H (blue), and Si (green) impurity profiles of sample A (**A**) and sample B (**B**). Note that the O peak with a density of 6 ×10^{21} cm^{-3} indicated by the arrow in (A) is absent in (B). The detection limits are 5 ×10^{16} cm^{-3} for C, 3×10^{17} cm^{-3} for O, 1 ×10^{17} cm^{-3} for Si, and 1 ×10^{18} cm^{-3} for H.

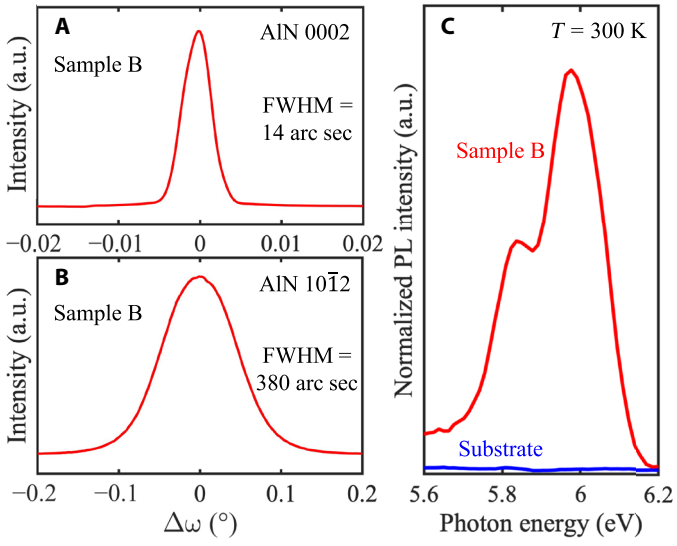

Fig. 9. Structural and optical properties of MBE-grown N-polar AlN. XRCs of sample B across AlN (**A**) (0002) and (**B**) (10$\bar{1}$2) reflections. (**C**) Room temperature PL spectra around the band-edge of AlN of sample B (red line) and a bare AlN template (blue line). Note that near band-edge PL emission peaks are only observed on sample B not on the bare AlN template.

For a feasibility study of N-polar device growth on N-polar AlN template, we grew GaN/AlGaN heterostructures on an N-polar AlN template with Al-assisted cleaning, where polarization-induced 2DEGs should be formed at the GaN/AlGaN interface, if the structure is N-polar. Temperature-dependent Hall effect measurements show *n*-type conductivity with an electron density of ~3.6 ×10^{13} cm^{-2}, which maintains down to 10 K and a room temperature electron mobility of ~190 cm^2 V^{-1}s^{-1} (see fig. S2). The measured 2DEG density matches with the calculated value of ~4.2×10^{13} cm^{-2} based on a self-consistent 1D Schrödinger-Poisson simulation. On the contrary, nominally, the same GaN/AlGaN heterostructures grown on an AlN template without Al-assisted cleaning shows insulating behavior, indicating the absence of such a high-density 2DEG.

DISCUSSION

MBE homoepitaxy of N-polar AlN is achieved on N-polar AlN templates. The in situ Al-assisted surface cleaning before MBE growth is found to be critical in preventing polarity inversion. The MBE-grown N-polar AlN, having a very smooth surface with parallel atomic steps, maintains the high structural quality of the substrate with no noticeable structural distortion or generation of dislocations at growth interface. The suppression of nonradiative recombination centers in the MBE-grown N-polar AlN epilayer is further revealed by the observation of clear room temperature near band-edge PL emission. These results suggest the great potential of MBE homoepitaxy for preparation of electronic-grade and optical-grade N-polar AlN.

MATERIALS AND METHODS

The samples in this study are prepared using MBE in a Veeco GENxplor MBE system equipped with a standard effusion cell for Al and a radio frequency plasma source for active N species. A KSA Instruments RHEED apparatus with a Staib electron gun operating at 14.5 kV and 1.45 A was used to in situ monitor the growth front. The substrates used in this study are ~160-nm-thick N-polar AlN/*c*-plane sapphire templates grown by sputtering followed by high-temperature face-to-face annealing. Details about the preparation of N-polar AlN templates can be found elsewhere (*16*). This cost-effective growth method can produce large-area N-polar AlN templates. After ex situ cleaning in acetone, isopropyl alcohol, and deionized water (each for 10 min), AlN templates with an area of 1 cm by 1 cm were mounted in indium-free holders, loaded into the MBE system, and outgassed at 200°C for 8 hours. Approximately 300-nm AlN layers were then grown under Al-rich condition at a substrate thermocouple temperature of 940°C with an Al BEP of ~7 ×10^{-7} torr and nitrogen plasma operating at 200 W with an N_2 gas flow rate of 1.95 standard cubic centimeter per minute. After growth, excess Al droplets were desorbed in situ at an elevated thermocouple temperature of 970°C before unloading.

The surface morphologies of the grown samples were characterized by AFM in an Asylum Research Cypher ES setup. XRD using a PANalytical X'Pert Pro setup at 45 kV and 40 mA with the Cu Kα1 radiation (1.5406 Å) and Raman spectroscopy using a 532-nm laser confocal microscope equipped with a 1800-mm^{-1} diffraction grating were also used for structural characterization. The microstructure of the samples was studied by TEM using a JEOL JEM-2100 instrument working at 200 kV. Cross-sectional STEM measurements were further performed to directly probe the polarity of the AlN layers using a JEOL ARM-200F system at an accelerating voltage of 200 kV. Before the (S)TEM characterization, thin cross-sectional and plan-view

specimens were prepared using a FEI Versa 3D DualBeam focused ion beam. SIMS was performed at EAG Laboratories to study impurity incorporation. Deep ultraviolet PL spectroscopy was used to probe the optical transitions in the N-polar AlN epilayer. Samples were excited from the top using a pulsed ArF excimer laser excitation at 193 nm with an energy of 2 mJ and a repetition rate of 100 Hz. The emitted light was collected from the side of the samples. Temperature-dependent Hall effect measurements were performed with indium dots as ohmic contacts under 1 T magnetic field to study the properties of 2DEGs.

SUPPLEMENTARY MATERIALS

Supplementary material for this article is available at https://science.org/doi/10.1126/sciadv.abo6408

REFERENCES AND NOTES

1. A. L. Hickman, R. Chaudhuri, S. J. Bader, K. Nomoto, L. Li, J. C. M. Hwang, H. Grace Xing, D. Jena, Next generation electronics on the ultrawide-bandgap aluminum nitride platform. *Semicond. Sci. Technol.* **36**, 044001 (2021).
2. B. Romanczyk, X. Zheng, M. Guidry, H. Li, N. Hatui, C. Wurm, A. Krishna, E. Ahmadi, S. Keller, U. K. Mishra, W-band power performance of SiN-passivated N-polar GaN deep recess HEMTs. *IEEE Electron Device Lett.* **41**, 349–352 (2020).
3. K. H. Hamza, D. Nirmal, A review of GaN HEMT broadband power amplifiers. *Int. J. Electron. Commun.* **116**, 153040 (2020).
4. M. H. Wong, Y. Pei, T. Palacios, L. Shen, A. Chakraborty, L. S. McCarthy, S. Keller, S. P. DenBaars, J. S. Speck, U. K. Mishra, Low nonalloyed Ohmic contact resistance to nitride high electron mobility transistors using N-face growth. *Appl. Phys. Lett.* **91**, 232103 (2007).
5. M. H. Wong, M. H. Wong, Y. Pei, R. Chu, S. Rajan, B. L. Swenson, D. F. Brown, S. Keller, S. P. Den Baars, J. S. Speck, U. K. Mishra, N-face metal-insulator-semiconductor high-electron-mobility transistors with AlN back-barrier. *IEEE Electron Device Lett.* **29**, 1101–1104 (2008).
6. J. Lemettinen, H. Okumura, T. Palacios, S. Suihkonen, N-polar AlN buffer growth by metal-organic vapor phase epitaxy for transistor applications. *Appl. Phys. Express* **11**, 101002 (2018).
7. T. Ito, R. Sakamoto, T. Isono, Y. Yao, Y. Ishikawa, N. Okada, K. Tadatomo, Growth and characterization of nitrogen-polar AlGaN/AlN heterostructure for high-electron-mobility transistor. *Phys. Status Solidi B* **257**, 1900589 (2020).
8. A. Hickman, R. Chaudhuri, S. J. Bader, K. Nomoto, K. Lee, H. G. Xing, D. Jena, High breakdown voltage in RF AlN/GaN/AlN quantum well HEMTs. *IEEE Electron Device Lett.* **40**, 1293–1296 (2019).
9. J. Lemettinen, N. Chowdhury, H. Okumura, I. Kim, S. Suihkonen, T. Palacios, Nitrogen-polar polarization-doped field-effect transistor based on $Al_{0.8}Ga_{0.2}N$/AlN on SiC with drain current over 100 mA/mm. *IEEE Electron Device Lett.* **40**, 1245–1248 (2019).
10. I. Smorchkova, L. Chen, T. Mates, L. Shen, S. Heikman, B. Moran, S. Keller, S. P. Den Baars, J. S. Speck, U. K. Mishra, AlN/GaN and (Al,Ga)N/AlN/GaN two-dimensional electron gas structures grown by plasma-assisted molecular-beam epitaxy. *J. Appl. Phys.* **90**, 5196 (2001).
11. S. Dasgupta, F. Wu, J. Speck, U. Mishra, Growth of high quality N-polar AlN (000$\bar{1}$) on Si (111) by plasma assisted molecular beam epitaxy. *Appl. Phys. Lett.* **94**, 151906 (2009).
12. O. Ledyaev, M. Pandikunta, S. Nikishin, N-polar AlN thin layers grown on Si (111) by plasma-assisted MBE. *Jpn. J. Appl. Phys.* **53**, 050306 (2014).
13. J. Lemettinen, H. Okumura, I. Kim, C. Kauppinen, T. Palacios, S. Suihkonen, MOVPE growth of N-polar AlN on 4H-SiC: Effect of substrate miscut on layer quality. *J. Cryst. Growth* **487**, 12–16 (2018).
14. T. Isono, T. Ito, R. Sakamoto, Y. Yao, Y. Ishikawa, N. Okada, K. Tadatomo, Growth of N-polar aluminum nitride on vicinal sapphire substrates and aluminum nitride bulk substrates. *Phys. Status Solidi B* **257**, 1900588 (2020).
15. H. Okumura, T. Kimoto, J. Suda, Growth of nitrogen-polar 2H-AlN on step-height-controlled 6H-SiC (000$\bar{1}$) substrate by molecular-beam epitaxy. *Jpn. J. Appl. Phys.* **51**, 02BH02 (2012).
16. K. Shojiki, K. Uesugi, S. Kuboya, H. Miyake, Reduction of threading dislocation densities of N-polar face-to-face annealed sputtered AlN on sapphire. *J. Cryst. Growth* **574**, 126309 (2021).
17. Z. Liu, Y. Guo, J. Yan, Y. Zeng, J. Wang, J. Li, Polarity tuning of crystalline AlN films utilizing trace oxygen involved sputtering and post-high-temperature annealing. *Appl. Phys. Express* **14**, 085501 (2021).
18. S. Keller, N. Fichtenbaum, F. Wu, G. Lee, S. P. DenBaars, J. S. Speck, U. K. Mishra, Effect of the nucleation conditions on the polarity of AlN and GaN films grown on C-face 6H-SiC. *Jpn. J. Appl. Phys.* **45**, L322–L325 (2006).
19. Y. Cho, C. S. Chang, K. Lee, M. Gong, K. Nomoto, M. Toita, L. J. Schowalter, D. A. Muller, D. Jena, H. G. Xing, Molecular beam homoepitaxy on bulk AlN enabled by aluminum-assisted surface cleaning. *Appl. Phys. Lett.* **116**, 172106 (2020).
20. K. Lee, Y.-J. Cho, L. J. Schowalter, M. Toita, H. G. Xing, D. Jena, Surface control and MBE growth diagram for homoepitaxy on single-crystal AlN substrates. *Appl. Phys. Lett.* **116**, 262102 (2020).
21. C. Wurm, E. Ahmadi, F. Wu, N. Hatui, S. Keller, J. Speck, U. Mishra, Growth of high-quality N-polar GaN on bulk GaN by plasma-assisted molecular beam epitaxy. *Solid State Commun.* **305**, 113763 (2020).
22. Y. P. Hong, J. H. Park, C. W. Park, H. M. Kim, D. K. Oh, B. G. Choi, S. K. Lee, K. B. Shim, Investigation of defects and surface polarity in AlN and GaN using wet chemical etching technique. *J. Korean Cryst. Growth Cryst. Technol.* **24**, 196–201 (2014).
23. R. Kirste, S. Mita, L. Hussey, M. P. Hoffmann, W. Guo, I. Bryan, Z. Bryan, J. Tweedie, J. Xie, M. Gerhold, R. Collazo, Z. Sitar, Polarity control and growth of lateral polarity structures in AlN. *Appl. Phys. Lett.* **102**, 181913 (2013).
24. L. Lu, Z. Y. Gao, B. Shen, F. J. Xu, S. Huang, Z. L. Miao, Y. Hao, Z. J. Yang, G. Y. Zhang, X. P. Zhang, J. Xu, D. P. Yu, Microstructure and origin of dislocation etch pits in GaN epilayers grown by metal organic chemical vapor deposition. *J. Appl. Phys.* **104**, 123525 (2008).
25. W. Guo, R. Kirste, I. Bryan, Z. Bryan, L. Hussey, P. Reddy, J. Tweedie, R. Collazo, Z. Sitar, KOH based selective wet chemical etching of AlN, $Al_xGa_{1-x}N$, and GaN crystals: A way towards substrate removal in deep ultraviolet-light emitting diode. *Appl. Phys. Lett.* **106**, 082110 (2015).
26. T. Akiyma, M. Uchino, K. Nakamura, T. Ito, S. Xiao, H. Miyake, Structural analysis of polarity inversion boundary in sputtered AlN films annealed under high temperatures. *Jpn. J. Appl. Phys.* **58**, SCCB30 (2019).
27. N. Stolyarchuk, T. Markurt, A. Courville, K. March, J. Zúñiga-Pérez, P. Vennéguès, M. Albrecht, Intentional polarity conversion of AlN epitaxial layers by oxygen. *Sci. Rep.* **8**, 14111 (2018).
28. M. Takeuchi, H. Shimizu, R. Kajitani, K. Kawasaki, T. Kinoshita, K. Takada, H. Murakami, Y. Kumagai, A. Koukitu, T. Koyama, S. F. Chichibu, Y. Aoyagi, Al- and N-polar AlN layers grown on c-plane sapphire substrates by modified flow-modulation MOCVD. *J. Cryst. Growth* **305**, 360–365 (2007).
29. H. Ye, G. Chen, Y. Zhu, S.-H. Wei, Asymmetry of adsorption of oxygen at wurtzite AlN (0001) and (000$\bar{1}$) surfaces: First-principles calculations. *Phys. Rev. B* **77**, 033302 (2008).
30. J. Li, K. Nam, M. Nakarmi, J. Lin, H. Jiang, Band-edge photoluminescence of AlN epilayers. *Appl. Phys. Lett.* **81**, 3365–3367 (2002).
31. M. Feneberg, R. A. Leute, B. Neuschl, K. Thonke, M. Bickermann, High-excitation and high-resolution photoluminescence spectra of bulk AlN. *Phys. Rev. B* **82**, 075208 (2010).
32. L. Romano, J. Northrup, M. O'keefe, Inversion domains in GaN grown on sapphire. *Appl. Phys. Lett.* **69**, 2394–2396 (1996).

Acknowledgments: We thank R. Page for critical reading of the manuscript. **Funding:** The authors at Cornell University acknowledge financial support from the Cornell Center for Materials Research (CCMR)—an NSF MRSEC program (no. DMR-1719875) for MBE growth; ULTRA, an Energy Frontier Research Center funded by the U.S. Department of Energy (DOE), Office of Science, Basic Energy Sciences (BES), under award no. DE-SC0021230 for material characterizations; and AFOSR grant no. FA9550-20-1-0148 for supporting collaborations in this work. This work uses the CESI Shared Facility partly sponsored by NSF no. MRI DMR-1631282 and Kavli Institute at Cornell (KIC). Y.H. acknowledges funding support from JSPS KAKENHI (grant number 19K15045). H.M. acknowledges funding support from MEXT "Program for Building Regional Innovation Ecosystems." **Author contributions:** Z.Z., H.G.X., D.J., and Y.C. conceived the research. Z.Z. grew the samples by MBE and conducted the AFM, XRD, Raman spectroscopy, and KOH etching experiments with help from Y.C. Y.H., T.T., and A.S. performed (S)TEM studies. Y.H. and H.M. performed the growth of the large-area N-polar AlN templates. Z.Z. and V.P. conducted PL measurements. Z.Z., D.J., and Y.C. wrote the manuscript with contribution from all authors. **Competing interests:** The authors declare that they have no competing interests. **Data and materials availability:** All data needed to evaluate the conclusions in the paper are present in the paper and/or the Supplementary Materials.

Submitted 16 February 2022
Accepted 26 July 2022
Published 9 September 2022
10.1126/sciadv.abo6408

ScienceAdvances

Molecular beam homoepitaxy of N-polar AlN: Enabling role of aluminum-assisted surface cleaning

Zexuan ZhangYusuke HayashiTetsuya ToheiAkira SakaiVladimir ProtasenkoJashan SinghalHideto MiyakeHuili Grace XingDebdeep JenaYongJin Cho

Sci. Adv., 8 (36), eabo6408. • DOI: 10.1126/sciadv.abo6408

Science Advances (ISSN) is published by the American Association for the Advancement of Science. 1200 New York Avenue NW, Washington, DC 20005. The title *Science Advances* is a registered trademark of AAAS.

Science Advances
AAAS

Supplementary Materials for

Molecular beam homoepitaxy of N-polar AlN: Enabling role of aluminum-assisted surface cleaning

Zexuan Zhang *et al.*

Corresponding author: Zexuan Zhang, zz523@cornell.edu; YongJin Cho, yongjin.cho@cornell.edu

Sci. Adv. **8**, eabo6408 (2022)
DOI: 10.1126/sciadv.abo6408

This PDF file includes:

Supplementary Text

Microstructures of the defects in AlN samples were studied using cross-sectional (S)TEM. The actual nature of the defects was identified using cross-sectional TEM (Fig. S1), where the Burgers vector $\boldsymbol{b}$ of threading dislocations are determined by adjusting the diffraction vector g using the $\boldsymbol{g}\cdot\boldsymbol{b}=0$ criterion. Non centrosymmetric reflection $\boldsymbol{g}=0002$ and $000\bar{2}$ were also used to detect any inversion domains which appear as contrast inversion in images taken with these diffraction vectors (*32*).

Temperature-dependent Hall-effect measurements reveal the presence of high-density polarization-induced two-dimensional electron gas (2DEG) at a N-polar $GaN/Al_{0.9}Ga_{0.1}N$ heterostructure (Fig. S2A) grown on N-polar AlN template after Al-assisted surface cleaning. The measured electron density of ~ 3.6×10^{13} cm^{-2} (Fig. S2C), which maintains down to 10 K, indicates its polarization-induced origin, and agrees with the calculated value of 4.2×10^{13} cm^{-2} based on a self-consistent 1D Schrödinger-Poisson simulation shown in Fig. S2B. Figure S2D shows the electron mobility as a function of temperature. The electron mobility increases monotonically with decreasing temperature from 190 $cm^2V^{-1}s^{-1}$ at 290 K to 240 $cm^2V^{-1}s^{-1}$ at 10 K, due to freeze-out of phonon scattering. On the other hand, nominally the same $GaN/Al_{0.9}Ga_{0.1}N$ heterostructure grown on N-polar AlN template without Al-assisted cleaning shows insulating behavior, indicating the absence of such a polarization-induced 2DEG.

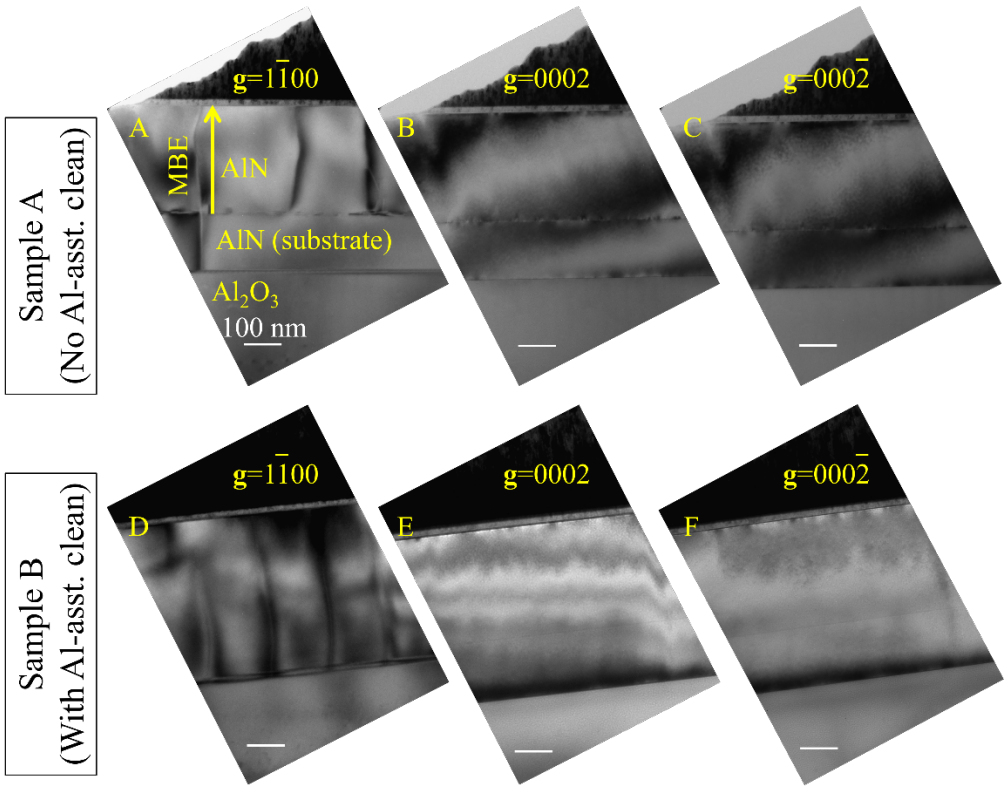

Fig. S1. Two-beam bright-field cross-sectional TEM images of AlN grown on AlN templates. (A to C) Sample A and (D to F) sample B near the <11$\bar{2}$0> zone axis with *g*=1$\bar{1}$00 (A and D), *g*=0002 (B and E) and *g*=000$\bar{2}$ (C and F).

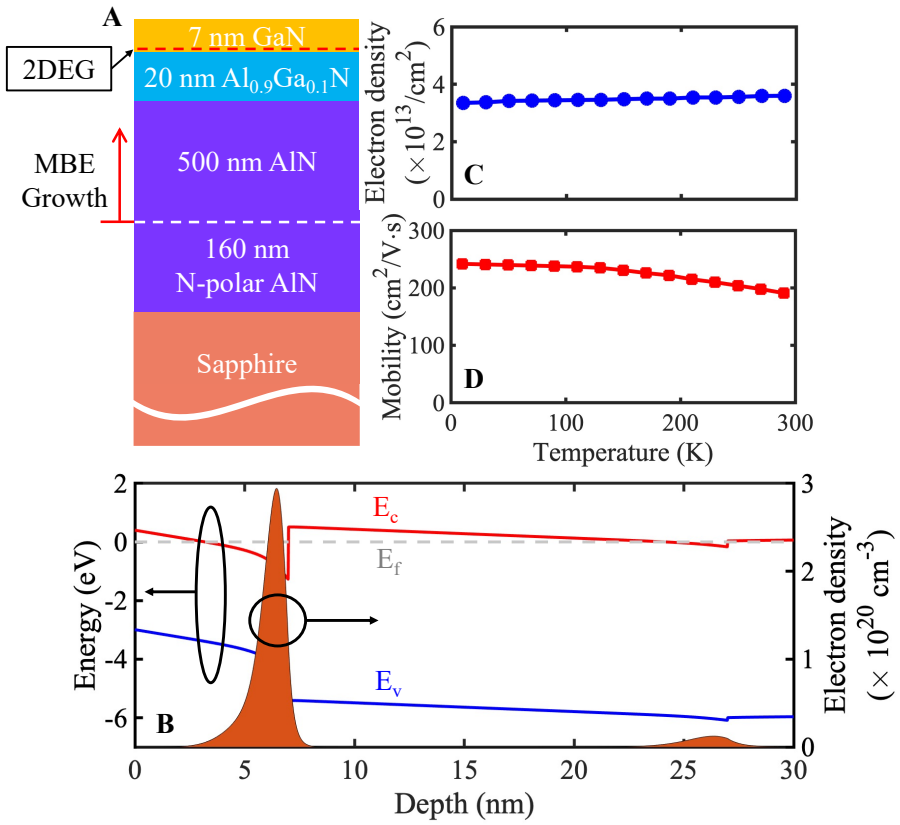

Fig. S2. GaN/$Al_{0.9}Ga_{0.1}N$ heterostructure grown on N-polar AlN template cleaned by Al-assisted deoxidation. (A) Schematic and (B) simulated energy band diagram of the structure. (C) Electron density and (D) Hall mobility as a function of temperature.

REFERENCES AND NOTES

1. A. L. Hickman, R. Chaudhuri, S. J. Bader, K. Nomoto, L. Li, J. C. M. Hwang, H. Grace Xing, D. Jena, Next generation electronics on the ultrawide-bandgap aluminum nitride platform. *Semicond. Sci. Technol.* **36**, 044001 (2021).

2. B. Romanczyk, X. Zheng, M. Guidry, H. Li, N. Hatui, C. Wurm, A. Krishna, E. Ahmadi, S. Keller, U. K. Mishra, W-band power performance of SiN-passivated N-polar GaN deep recess HEMTs. *IEEE Electron Device Lett.* **41**, 349–352 (2020).

3. K. H. Hamza, D. Nirmal, A review of GaN HEMT broadband power amplifiers. *Int. J. Electron. Commun.* **116**, 153040 (2020).

4. M. H. Wong, Y. Pei, T. Palacios, L. Shen, A. Chakraborty, L. S. McCarthy, S. Keller, S. P. DenBaars, J. S. Speck, U. K. Mishra, Low nonalloyed Ohmic contact resistance to nitride high electron mobility transistors using N-face growth. *Appl. Phys. Lett.* **91**, 232103 (2007).

5. M. H. Wong, M. H. Wong, Y. Pei, R. Chu, S. Rajan, B. L. Swenson, D. F. Brown, S. Keller, S. P. Den Baars, J. S. Speck, U. K. Mishra, N-face metal-insulator-semiconductor high-electron-mobility transistors with AlN back-barrier. *IEEE Electron Device Lett.* **29**, 1101–1104 (2008).

6. J. Lemettinen, H. Okumura, T. Palacios, S. Suihkonen, N-polar AlN buffer growth by metal-organic vapor phase epitaxy for transistor applications. *Appl. Phys. Express* **11**, 101002 (2018).

7. T. Ito, R. Sakamoto, T. Isono, Y. Yao, Y. Ishikawa, N. Okada, K. Tadatomo, Growth and characterization of nitrogen-polar AlGaN/AlN heterostructure for high-electron-mobility transistor. *Phys. Status Solidi B* **257**, 1900589 (2020).

8. A. Hickman, R. Chaudhuri, S. J. Bader, K. Nomoto, K. Lee, H. G. Xing, D. Jena , High breakdown voltage in RF AlN/GaN/AlN quantum well HEMTs. *IEEE Electron Device Lett.* **40**, 1293–1296 (2019).

9. J. Lemettinen, N. Chowdhury, H. Okumura, I. Kim, S. Suihkonen, T. Palacios, Nitrogen-polar polarization-doped field-effect transistor based on $Al_{0.8}Ga_{0.2}N$/AlN on SiC with drain current over 100 mA/mm. *IEEE Electron Device Lett.* **40**, 1245–1248 (2019).

10. I. Smorchkova, L. Chen, T. Mates, L. Shen, S. Heikman, B. Moran, S. Keller, S. P. Den Baars, J. S. Speck, U. K. Mishra, AlN/GaN and (Al,Ga)N/AlN/GaN two-dimensional electron gas structures grown by plasma-assisted molecular-beam epitaxy. *J. Appl. Phys.* **90**, 5196 (2001).

11. S. Dasgupta, F. Wu, J. Speck, U. Mishra, Growth of high quality N-polar AlN $(000\bar{1})$ on Si (111) by plasma assisted molecular beam epitaxy. *Appl. Phys. Lett.* **94**, 151906 (2009).

12. O. Ledyaev, M. Pandikunta, S. Nikishin, N-polar AlN thin layers grown on Si (111) by plasma-assisted MBE. *Jpn. J. Appl. Phys.* **53**, 050306 (2014).

13. J. Lemettinen, H. Okumura, I. Kim, C. Kauppinen, T. Palacios, S. Suihkonen, MOVPE growth of N-polar AlN on 4H-SiC: Effect of substrate miscut on layer quality. *J. Cryst. Growth* **487**, 12–16 (2018).

14. T. Isono, T. Ito, R. Sakamoto, Y. Yao, Y. Ishikawa, N. Okada, K. Tadatomo, Growth of N-polar aluminum nitride on vicinal sapphire substrates and aluminum nitride bulk substrates. *Phys. Status Solidi B* **257**, 1900588 (2020).

15. H. Okumura, T. Kimoto, J. Suda, Growth of nitrogen-polar 2H-AlN on step-height-controlled 6H-SiC $(000\bar{1})$ substrate by molecular-beam epitaxy. *Jpn. J. Appl. Phys.* **51**, 02BH02 (2012).

16. K. Shojiki, K. Uesugi, S. Kuboya, H. Miyake, Reduction of threading dislocation densities of N-polar face-to-face annealed sputtered AlN on sapphire. *J. Cryst. Growth* **574**, 126309 (2021).

17. Z. Liu, Y. Guo, J. Yan, Y. Zeng, J. Wang, J. Li, Polarity tuning of crystalline AlN films utilizing trace oxygen involved sputtering and post-high-temperature annealing. *Appl. Phys. Express* **14**, 085501 (2021).

18. S. Keller, N. Fichtenbaum, F. Wu, G. Lee, S. P. DenBaars, J. S. Speck, U. K. Mishra , Effect of the nucleation conditions on the polarity of AlN and GaN films grown on C-face 6H-SiC. *Jpn. J. Appl. Phys.* **45**, L322–L325 (2006).

19. Y. Cho, C. S. Chang, K. Lee, M. Gong, K. Nomoto, M. Toita, L. J. Schowalter, D. A. Muller, D. Jena, H. G. Xing, Molecular beam homoepitaxy on bulk AlN enabled by aluminum-assisted surface cleaning. *Appl. Phys. Lett.* **116**, 172106 (2020).

20. K. Lee, Y.-J. Cho, L. J. Schowalter, M. Toita, H. G. Xing, D. Jena, Surface control and MBE growth diagram for homoepitaxy on single-crystal AlN substrates. *Appl. Phys. Lett.* **116**, 262102 (2020).

21. C. Wurm, E. Ahmadi, F. Wu, N. Hatui, S. Keller, J. Speck, U. Mishra , Growth of high-quality N-polar GaN on bulk GaN by plasma-assisted molecular beam epitaxy. *Solid State Commun.* **305**, 113763 (2020).

22. Y. P. Hong, J. H. Park, C. W. Park, H. M. Kim, D. K. Oh, B. G. Choi, S. K. Lee, K. B. Shim, Investigation of defects and surface polarity in AlN and GaN using wet chemical etching technique. *J. Korean Cryst. Growth Cryst. Technol.* **24**, 196–201 (2014).

23. R. Kirste, S. Mita, L. Hussey, M. P. Hoffmann, W. Guo, I. Bryan, Z. Bryan, J. Tweedie, J. Xie, M. Gerhold, R. Collazo, Z. Sitar , Polarity control and growth of lateral polarity structures in AlN. *Appl. Phys. Lett.* **102**, 181913 (2013).

24. L. Lu, Z. Y. Gao, B. Shen, F. J. Xu, S. Huang, Z. L. Miao, Y. Hao, Z. J. Yang, G. Y. Zhang, X. P. Zhang, J. Xu, D. P. Yu , Microstructure and origin of dislocation etch pits in GaN epilayers grown by metal organic chemical vapor deposition. *J. Appl. Phys.* **104**, 123525 (2008).

25. W. Guo, R. Kirste, I. Bryan, Z. Bryan, L. Hussey, P. Reddy, J. Tweedie, R. Collazo, Z. Sitar, KOH based selective wet chemical etching of AlN, $Al_xGa_{1-x}N$, and GaN crystals: A way towards substrate removal in deep ultraviolet-light emitting diode. *Appl. Phys. Lett.* **106**, 082110 (2015).

26. T. Akiyma, M. Uchino, K. Nakamura, T. Ito, S. Xiao, H. Miyake, Structural analysis of polarity inversion boundary in sputtered AlN films annealed under high temperatures. *Jpn. J. Appl. Phys.* **58**, SCCB30 (2019).

27. N. Stolyarchuk, T. Markurt, A. Courville, K. March, J. Zúñiga-Pérez, P. Vennéguès, M. Albrecht , Intentional polarity conversion of AlN epitaxial layers by oxygen. *Sci. Rep.* **8**, 14111 (2018).

28. M. Takeuchi, H. Shimizu, R. Kajitani, K. Kawasaki, T. Kinoshita, K. Takada, H. Murakami, Y. Kumagai, A. Koukitu, T. Koyama, S. F. Chichibu, Y. Aoyagi , Al- and N-polar AlN layers grown on c-plane sapphire substrates by modified flow-modulation MOCVD. *J. Cryst. Growth* **305**, 360–365 (2007).

29. H. Ye, G. Chen, Y. Zhu, S.-H. Wei, Asymmetry of adsorption of oxygen at wurtzite AlN (0001) and $(000\bar{1})$ surfaces: First-principles calculations. *Phys. Rev. B* **77**, 033302 (2008).

30. J. Li, K. Nam, M. Nakarmi, J. Lin, H. Jiang, Band-edge photoluminescence of AlN epilayers. *Appl. Phys. Lett.* **81**, 3365–3367 (2002).

31. M. Feneberg, R. A. Leute, B. Neuschl, K. Thonke, M. Bickermann, High-excitation and high-resolution photoluminescence spectra of bulk AlN. *Phys. Rev. B* **82**, 075208 (2010).

32. L. Romano, J. Northrup, M. O'keefe, Inversion domains in GaN grown on sapphire. *Appl. Phys. Lett.* **69**, 2394–2396 (1996).